An active plasma beam dump for compact deceleration of electron beams

May 11, 2020

Xueying Wang

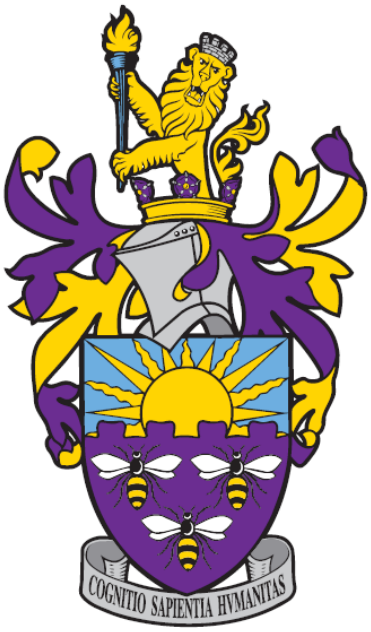

School of Physics and Astronomy

University of Manchester

Abstract

This report represents the second-semester MPhys project based on plasma beam deceleration technology research. In the last report, we studied issues related to a passive plasma beam dump. In this report, we mainly focus on the active scheme, in which a laser pulse is injected into the plasma before the electron beam to be processed. The purpose of introducing the laser is to flatten the net wakefield and extract the energy of the particles in the beam head. Theoretical models and simulations show the special advantages of active PBDs and make up for the limitations of the passive scheme. Based on the plasma fluid theory, an analytical model was established. A plasma channel is used to solve the dephasing problem, and then we can assume that the laser pulse will not change along the propagation distance. The energy loss function is also extended to the discussion of active schemes. Then, we apply the results to EuPRAXIA and BNL parameters, showing the broad prospects for further research. The FBPIC code is also used to simulate laser-plasma, beam-plasma interaction, and energy extraction. It predicts that active PBDs can slow down particles in a shorter distance compared to the passive scheme.

Keywords: Laser-driven plasma wakefield, Active plasma beam dump, FBPIC

Contents

1 Introduction

1.1 Introduction to plasma beam dump

In contemporary high-energy physics research, ultra-relativistic particles are usually produced then to collide with each other or with the target material to obtain sub-atomic particles. After the reactions, a beam dump must be used to slow down the used particles that still contain large energy. In addition to scientific research, there are many other fields, such as industrial, medical, and other practical applications, as long as high-energy beams are used, a beam dump needs to be employed. Conventionally, scientists use dense materials, such as metal, graphite, or water, to dump used energetic beams to a safety regime, preventing from releasing hazards to the environment. The dump mechanism is mainly based on the collisions between the external highly-energetic particles with the electrons inside the dump material. Due to its relatively low stopping power which is determined by the Bohr-Fermi-Bethe-Bloch theory [1], the conventional dumps are usually of large volume and surrounded by thick concrete. For next-generation plasma wakefield-based accelerators, it is very cumbersome to utilize the large dump sections in reality, and contrary to the request for a greener and cheaper device. Besides, it would create a large amount of radiation and heat as a result of excessive binary collisions, and if not dealt with properly, the directly released radiation would cause great damage to the operating systems as well as the external environment. So in the real experiments, there are always a cooling system and other additional sections to cope with the radionuclides [2], leading to an even larger footprint of the dump section. Nowadays, the trend for obtaining ultra-relativistic beams with higher and higher energies is global, while how to dispose of the used beam in a shorter distance, and at the same time more safely, is an unavoidable problem. To overcome the limitations of the conventional beam, enlightened by the schemes of plasma wakefield-based accelerators, scientists have raised the concept of plasma beam dumps (PBD).

In 2010, H. C. Wu. and T. Tajima first proposed the idea of the plasma beam dump to decelerate charged particles [3], taking the advantages of the large amplitude of wakefield excited by an external electron or proton beam or a laser pulse. Another advantage of PBD is that due to the lack of collisions in the low-density plasma, there is little radionuclide production. The electrons in plasma can move collectively under extrinsic perturbation, producing a significant oscillating electron-density wave which is called a wakefield. In their calculations, the typical ratio between the stopping powers of plasma and conventional beam dump can be up to 10^3, which means that the PBD can decelerate the particles in a distance that is shorter than the traditional three orders of magnitude. The plasma wakefield-based accelerators (PWFA) are of the same physics as in PBD except for the different phase position of the beam [4] [5] [6]. The feasibility of the accelerators has already been demonstrated in simulations and experiments. For example, an experiment in SLAC used an electron-driven wakefield accelerator to achieve an energy doubling in an 85 cm-long plasma, accelerating an electron beam from 42 GeV to 84 GeV [7]. The advantages and the demonstration of PWFA show a promising prospect for researching and maturing the technology of PBD.

Currently, there are two schemes of PBD. The first is called the passive scheme, where a single electron bunch is used to excite a wakefield inside the plasma, and subsequently, this wakefield can decelerate the electrons sitting in the middle and tail of the beam. The second one is called the active scheme, where a laser pulse is added prior to the electron beam to compensate for the limitations in the former case. In the previous report, we mainly concentrated on the passive scheme, while in this report we will focus on the active one.

1.2 Summary of the previous report

This section aims to briefly summarize the material in the previous report. An analytical model of plasma wakefield excitation by an electron beam, which is occurred in a passive PBD, is described through plasma fluid theory. In other words, in the cold plasma limit, the response of plasma electrons to extrinsic irritation can be depicted by treating these electrons as plasma fluid elements. The wakefield can be calculated through perturbation theory, where we have assumed that the ions stay stationary as the driven beam propagates,

but the electrons would oscillate sinusoidally with the frequency that is called the plasma frequency:

$$\omega_p = \sqrt{\frac{n_0 e^2}{\epsilon_0 m_e}}, \tag{1.1}$$

where n_0 is plasma electron density, e is electron charge, ϵ_0 is vacuum permittivity, m_e is electron mass. Then with the calculation of the electron perturbated density, the longitudinal and transverse wakefield can be calculated, where the longitudinal direction z means the direction of the beam propagation axis, while the transverse direction is perpendicular to z-axis, i.e. radially. Using the typical EuPRAXIA beam parameters [8], we plotted the wakefield shape in 1-dimension, as depicted in Figure 1(a). The horizontal axis in the figure is $k_p\xi$ where $k_p = \omega_p/c$ the plasma wavenumber, and $\xi = z - ct$ is the representation in the comoving frame with c the speed of light and t the propagation time. n_b is the Gaussian beam density distribution, which is normalized with respect to the plasma density in the figure. The wakefield is also normalized by $E_0 = k_p m_e c^2/e$, the cold non-relativistic wave-breaking field. The positive wakefield corresponds to a decelerating phase for electrons, and negative wakefield is related to the accelerating phase. Hence, to realize the goal of extracting the energy of used electron beam out, the beam should be short enough to be totally entirely in the decelerating phase. This requirement is well suited for bunches obtained from PWFA due to the matching of wavelengths between the beam and the wakefield.

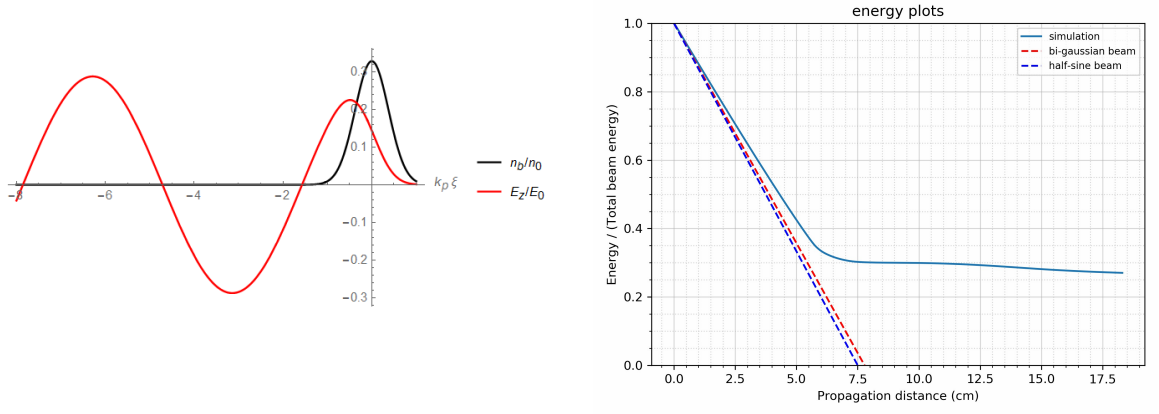

(a) (b)

Figure 1: (a) shows longitudinal distribution of one-dimensional normalized Gaussian beam density and corresponding wakefields in theoretical prediction under EuPRAXIA parameters. (b) shows comparison of energy loss caused by matched half-sine and Gaussian beams respectively and FBPIC numerical Gaussian beam result with application to EuPRAXIA.

Satisfying the fitting conditions, we then calculated the work done by the electric field on the electron beam to obtain an energy loss function with propagation distance, which will show a linear decline slope of the total energy, as shown in Figure 1(b). It can be seen that, after a certain propagation distance, the theoretical prediction contradicts the simulation result due to the significant effect called saturation. After a period of propagation, the electrons that witness the maximum deceleration gradient will first reach the non-relativistic limit, so suddenly they will fall behind until reaching the acceleration phase, and then form a secondary peak. The process of re-acceleration will saturate the total energy loss, which is also an important limitation on passive PBD.

The Fourier-Bessel Particle In Cell (FBPIC) code [9] has been used to simulate the evolution of the beam during propagation. The numerical method shows the saturation effect more directly, as shown in Figure 2. To bring down the saturation effect and slow down the beam, we tried various tailored plasma density profiles to further promote energy extraction. It can be seen from the equation (1.1) that the plasma frequency, and the plasma wavelength $\lambda_p = 2\pi c/\omega_p$, are directly determined by the plasma density. Therefore, increasing

or reducing the plasma density can change the plasma wavelength to extend or shorten the deceleration or defocusing state, respectively. In this operation, the main method of reducing the saturation effect is to expel the reaccelerated electrons through the transverse defocusing effect. Simulations have shown an improvement in the passive PBD scheme using tailored plasma density profiles according to the previous report.

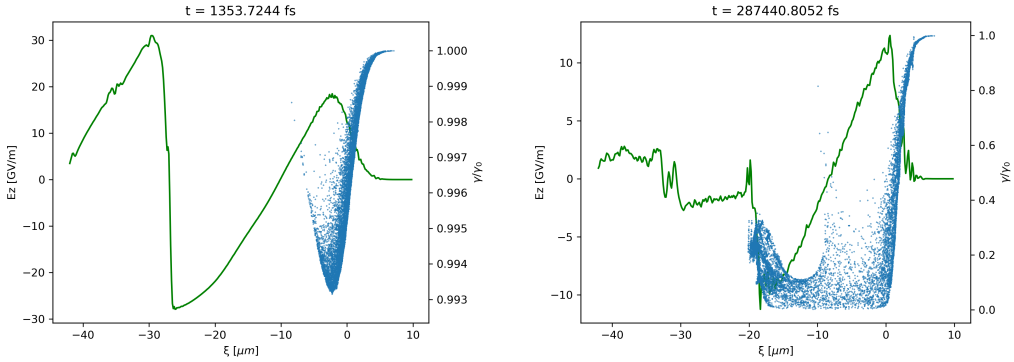

(a) (b)

Figure 2: FBPIC simulations on beams and their respective longitudinal wakefields under EuPRAXIA parameters. The green lines represent the longitudinal wakefield on-axis (r = 0), and the blue dots stand for particle positions in phase space. (a) represents the deceleration process at $t = 1354$ fs, equivalent propagation distance $s_1 = 0.04$ cm. (b) represents the reaceleration process at $t = 287441$ fs, corresponding to $s_2 = 8.6$ cm.

1.3 Active plasma beam dump

For passive PBD, in addition to the saturation problem, another disadvantage is that it cannot slow down the electrons located near the beam head. Due to the limited response time of the wakefield to the excitation, the amplitude of the electric field is close to zero at the beginning. To remedy these limitations, scientists have proposed the active scheme which was inspired by a laser-driven wakefield accelerator (LPA) [10]. A laser pulse is used to drive the wakefield before electrons arrive. As the laser propagates in the plasma, the ponderomotive force released by the laser pulse will expel the plasma electrons out, while the ions stay in rest. The ponderomotive force is a nonlinear force that a charged particle experiences in an inhomogeneous oscillating electromagnetic field. After the laser pulse, the electrons will witness the attraction of the ions, so they will be pushed back and thereafter form a wakefield [11]. The mechanism in laser-driven plasma wake results in its high acceleration gradient, which is also the concept of the laser plasma accelerator first proposed by T. Tajima in 1979 [4]. Thereafter the beam-driven (LWFA) and proton-driven plasma wakefield accelerator (PDPWA) have been put forward and researched. LPA is the most mature technology among the three. And it has been demonstrated many times experimentally, for example, in 2019, LBNL used LPA to accelerate electrons to 7.8 GeV in just 20 cm, showing an average accelerating gradient of 39 GeV/m [12]. Nowadays, other solutions to make up for the shortcomings of LPA are being studied, like using multi-pulse LPA to reduce the laser power and increase the repetition rate [13]. With the development of laser technology, LPA will gain further enhancement for future applications in reality.

In LPA, the electrons to be accelerated come from the background plasma or external injection. For simplification of the experimental operation, if we aim to take advantage of the self-injection effects and then accelerate these trapped electrons, the laser power requirement is relatively high for the sake of producing a bubble regime, i.e. expelling all electrons out behind the laser [11]. However, in the deceleration, the trapping of plasma electrons effect must be avoided as the aim is to extract the beam energy out. Thus the laser strength should be approximately equal to or less than 1, which is also beneficial to reducing laser energy consumption.

For the beam dump, if the phase difference between the laser pulse and the electron beam is appropri-

ately selected, the total wakefield generated by the combination of laser driving and electron beam driving can be flattened. Therefore, the energy extraction process can occur more uniformly, avoiding the saturation problem. In principle, all energy, including the electron energy at the head of the electron beam, can be transferred to the plasma, and then the used electron beam is completely disposed of. Besides, in the case of using laser pulses, if coherently superposed with the beam, the amplitude of the wakefield is larger than in the case of only the beam drive, resulting in a shorter deceleration distance. When adding laser pulses to a passive scheme, there are many experimental difficulties, such as calibrating the laser to the plasma channel, diffraction and depletion issues, and the selection and control of phase differences. At the same time, this will require additional laser energy consumption, which is not as environmentally friendly as the passive scheme. Despite many inconveniences and disadvantages, it is still worth studying the feasibility of active PBD.

1.4 Outline of report

This report details the work done in a full-year MPhys project as a continuous work from the previous report. We will concentrate on the theoretical model establishment and numerical simulation on the active plasma beam dump based on plasma wakefield excitation and passive scheme simulation presented in the last report. In Chapter 2, the mechanism for laser-driven plasma wakefield will be discussed analytically and the deterministic expressions for the electromagnetic field in the plasma will be derived. Then the energy loss function will be obtained through the same method as in the passive scheme while taking into account the combined effects of laser driving and beam driving. In Chapter 3, the FBPIC code will be used to simulate the beam and energy evolution as the laser propagates in a preformed channel.

2 Theoretical model and applications

2.1 Summary on beam-driven wakefield

In the previous report, we have derived the expressions for beam-driven wakefield from plasma fluid theory and perturbation theory. To discuss the active PBD where the wakefield is a combination of both laser and beam driving, we summarize the beam-driven result below. The electron beam is assumed to be 2D cylindrical symmetric, and the wakefield can be divided into the longitudinal and transverse direction. The longitudinal component is

$$E_{zb}(\xi, r) = -4\pi k_p^2 \int_{\infty}^{\xi} \cos(k_p(\xi - \xi'))d\xi' \int_0^{\infty} G(r, r')n_b(r', \xi')r'dr', \tag{2.1}$$

where the variable ξ is a representation in the comoving frame with the propagating beam with $\xi = z - vt$, where v is the velocity of the beam which is near the speed of light c. Another key parameter $k_p = \omega_p/c$ is plasma wavenumber, i.e. the plasma frequency, which is directly determined by the plasma density. The $G(r, r')$ in equation (2.1) is the Green function for the integral with I_0 and K_0 being the zeroth-order modified Bessel functions of the first and second kind, respectively:

$$\begin{aligned} G(r, r') &= -I_0(k_p r)K_0(k_p r')\Theta(r' - r) - I_0(k_p r')K_0(k_p r)\Theta(r - r') \\ &= -I_0(k_p r_<)K_0(k_p r_>), \end{aligned} \tag{2.2}$$

where $r_<$ means the smaller one between r and r', while $r_>$ means the larger one.
Under proper matching conditions, the behavior of a half-sinusoidal beam is very similar to a Gaussian beam. Even if the Gaussian beam is more realistic, using the half-sine beam shape is simpler in the calculation process. This is why we use the half-sine beam shape in the active scheme, because the wakefield expressions deem to be much more complicated. For a Gaussian beam, its density distribution is

$$n_b(\xi, r) = n_b exp\left(-\frac{\xi^2}{2\sigma_\xi^2}\right) exp\left(-\frac{r^2}{2\sigma_r^2}\right), \tag{2.3}$$

where σ_ξ and σ_r are axial and radial deviations respectively. And for a half-sine beam,

$$n_b(\xi, r) = n_b \sin\left(\frac{\pi\xi}{L}\right)\left(1 - \frac{r^2}{r_b^2}\right), \tag{2.4}$$

where L and r_b limits the distribution of the beam, i.e. the beam density is zero outside the regime $0 < \xi < L$ and $0 < r < r_b$. If just considering 1D geometry, the matching condition [21], i.e. the number of particles inside the beams with different profiles should be equal, gives

$$L = \frac{\pi^{3/2}}{\sqrt{2}}\sigma_\xi. \tag{2.5}$$

Then for a half-sine beam, the 1D wakefield expression is calculated through equation (2.1), represented in equation (2.6). This expression will be used in the discussion of energy loss calculation in active PBD directly.

$$\frac{E_{zb}^{HS}}{E_0} = \begin{cases} \frac{\pi k_p L(n_b/n_0)}{\pi^2 - k_p^2 L^2}\left(\cos(k_p(L - \xi)) + cos(\frac{\pi\xi}{L})\right) & 0 \le \xi \le L, \\ \frac{\pi k_p L(n_b/n_0)}{\pi^2 - k_p^2 L^2}\left(\cos(k_p(L - \xi)) + cos(k_p\xi)\right) & \xi < 0. \end{cases} \tag{2.6}$$

2.2 Plasma density perturbation

For the simplification of discussion, we consider non-evolving laser pulse as it propagates in an uniform plasma. It is convenient to use normalized electrostatic and vector potential, respectively.

$$\phi = \frac{e\Phi}{m_e c^2}, \tag{2.7}$$

$$\boldsymbol{a} = \frac{e\boldsymbol{A}}{m_e c^2}, \tag{2.8}$$

with $\boldsymbol{E} = -\nabla\Phi - \partial\boldsymbol{A}/\partial t$ and $\boldsymbol{B} = \nabla \times \boldsymbol{A}$. As we have discussed previously, in the deceleration process the self-injection effect should be avoided. Hence, the discussions should lie in the linear limit where $|\boldsymbol{a}| \ll 1$.

2.2.1 Ponderomotive force

In laser-driven wakefield, it is the ponderomotive force released from the electromagnetic field of the laser to drive the plasma wave. Treating plasma as fluid elements, the Lorentz force equation can be expressed as

$$\frac{d\boldsymbol{p}}{dt} = -e\left[\boldsymbol{E} + \frac{1}{c}(\boldsymbol{v} \times \boldsymbol{B})\right], \tag{2.9}$$

where the total derivative to time is a combination of a partial derivative to time and a velocity term according to the fluid theory

$$\frac{d}{dt} = \frac{\partial}{\partial t} + (\boldsymbol{v} \cdot \nabla).$$

The quiver momentum is defined as $\boldsymbol{p}_q = m_e c\boldsymbol{a}$, and satisfying $\partial\boldsymbol{p}_q/\partial t = -e\boldsymbol{E}$. Now considering the perturbation $\boldsymbol{p} = \boldsymbol{p}_q + \delta\boldsymbol{p}$, together with equation (2.9) and the non-relativistic condition $p_q = m_e\boldsymbol{v}$, we can obtain the following expression for the perturbation term [15]

$$\frac{d\delta\boldsymbol{p}}{dt} = -\left[\frac{\boldsymbol{p}_q}{m_e} \cdot \nabla\right]\boldsymbol{p}_q - \boldsymbol{p}_q \times (c\nabla \times \boldsymbol{a}) = -m_e c^2 \nabla\left(\frac{a^2}{2}\right). \tag{2.10}$$

The last term of equation (2.10) is defined as the 3D ponderomotive foce in the linear limit, i.e.

$$\boldsymbol{F}_p = -m_e c^2 \nabla\left(\frac{a^2}{2}\right). \tag{2.11}$$

2.2.2 Plasma density perturbation

Considering plasma fluid theory, the Lorentz force equation can be expressed as

$$m_e\left[\frac{\partial\boldsymbol{v}}{\partial t} + (\boldsymbol{v} \cdot \boldsymbol{\nabla})\boldsymbol{v}\right] = q(\boldsymbol{E} + \boldsymbol{v} \times \boldsymbol{B}), \tag{2.12}$$

where $\boldsymbol{v}$ is the velocity of the plasma electrons, $\boldsymbol{E}$ and $\boldsymbol{B}$ are electric and magnetic field. The continuity equation and Gauss's equation can be expressed as

$$\frac{\partial n_e}{\partial t} + \boldsymbol{\nabla} \cdot (n_e\boldsymbol{v}) = 0, \tag{2.13}$$

$$\epsilon_0\boldsymbol{\nabla} \cdot \boldsymbol{E} = -e(n_e - n_i), \tag{2.14}$$

where n_e and n_i are electron and ion density, respectively.

When the plasma wave is generated by a laser pulse, its 1D fluid equations in non-relativistic regime can be linearized through

$$v_\perp = a \cdot c, \tag{2.15}$$
$$n_i = n_0, \tag{2.16}$$
$$n_e = n_0 + \delta n_e, \tag{2.17}$$

where a is the laser strength, and n_0 is the unperturbed plasma density, while δn_e is the perturbation term with the assumption that the ions stay unperturbed under external effects. The equation (2.15) can be derived through the definition of the quiver momentum $p_\perp = m_e ca$, then in the non-relativistic limit $p_\perp = m_e v_\perp$,

thus obtaining the relationship between $v_\perp$ and a. The subscript $\perp$ indicates the direction perpendicular to the propagation axis of the laser. Ignoring the magnetic field, then the linearized fluid equations can be expressed as

$$m_e \frac{\partial v}{\partial t} + eE = -\frac{1}{2} m_e c^2 \frac{\partial a^2}{\partial x}, \tag{2.18}$$

$$n_0 \frac{\partial v}{\partial x} = -\frac{\partial \delta n_e}{\partial t}, \tag{2.19}$$

$$\frac{\partial E}{\partial x} = -\frac{e \delta n_e}{\epsilon_0}. \tag{2.20}$$

Taking the derivative of equation (2.18) with respect to x, and equation (2.19) with respect to t, and through substitution and calculations, we can obtain

$$\left(\frac{\partial^2}{\partial t^2} + \omega_p^2 \right) \delta n_e = \frac{n_0 c^2}{2} \frac{\partial^2 a^2}{\partial x^2}, \tag{2.21}$$

where we have substituted the definition of ω_p by equation (1.1).

Usually we will discuss the problems in the comoving frame, where $\xi = x - ct, \tau = t$. Considering quasi-static approximation, which states that the travelling wave appears static in the comoving frame, i.e. changing gradually in time compared to the spatial scale, hence, $\partial/\partial\tau = 0$, and subsequently $\partial/\partial t = -c\partial/\partial\xi$, $\partial/\partial x = \partial/\partial\xi$. Then the oscillating equation of the perturbed density(2.21) can be transferred into the form

$$\left(\frac{\partial^2}{\partial \xi^2} + k_p^2 \right) \delta n_e = \frac{n_0}{2} \frac{\partial^2 a^2}{\partial \xi^2}. \tag{2.22}$$

Extending the discussion to 3D, we can obtain the density perturbation equation of plasma waves generated in an initially uniform plasma. The equation (2.21) can be transformed into the 3D form as

$$\left(\frac{\partial^2}{\partial t^2} + \omega_p^2 \right) \frac{\delta n_e}{n_0} = c^2 \nabla^2 \left(\frac{a^2}{2} \right). \tag{2.23}$$

The Green function for solving the partial derivative equation (2.23) is

$$G(t, t') = \Theta(t - t') \frac{\sin\left[\omega_p (t - t')\right]}{\omega_p}.$$

Therefore, the solution to equation (2.23) can be obtained and expressed as

$$\frac{\delta n}{n_0} = \frac{c^2}{\omega_p} \int_0^t dt' \sin[\omega_p (t - t')] \nabla^2 \left[\frac{a^2(r', t')}{2} \right]. \tag{2.24}$$

2.2.3 Unified equations for beam and laser-driven wakefields

From Maxwell equations, we can obtain the wave equation for the electric field, i.e.

$$\nabla^2 \boldsymbol{E} - \frac{1}{c^2} \frac{\partial^2 \boldsymbol{E}}{\partial t^2} = \frac{4\pi}{c^2} \frac{\partial \boldsymbol{j}}{\partial t} + 4\pi \nabla \rho, \tag{2.25}$$

where the current $\boldsymbol{j} = \boldsymbol{j}_b + \boldsymbol{j}_p$ relates to the sum of beam and plasma electron current, characterized by subscripts b and p respectively, as well as the change in the charge density $\rho = \rho_b + \rho_p$. Considering the perturbation $n = n_0 + \delta n$, $\boldsymbol{v} = \boldsymbol{v}_0 + \delta \boldsymbol{v}$, where the unperturbed velocity should equal to zero. Hence, in the first-order perturbation theory, the current should satisfy $\boldsymbol{J} = qn\boldsymbol{v} \approx fqn_0 \delta \boldsymbol{v}$. For the beam current, its derivative of time should be

$$\frac{\partial \boldsymbol{J}_b}{\partial t} \approx -n_0 ec \frac{\partial}{\partial t} \left(\frac{n_b}{n_0} \right). \tag{2.26}$$

While for the plasma electron current, according to the Lorentz force equation (2.9), the velocity satisfies

$$\frac{d\boldsymbol{v}_p}{dt} \approx -\frac{e}{m}\boldsymbol{E} - c^2\frac{\partial}{\partial z}\left(\frac{a^2}{2}\right)\hat{\boldsymbol{e}}_z. \tag{2.27}$$

Therefore,

$$\frac{\partial \boldsymbol{J}_p}{\partial t} = \frac{n_0 e^2}{m}\boldsymbol{E} + n_0 e c^2\frac{\partial}{\partial z}\left(\frac{a^2}{2}\right)\hat{\boldsymbol{e}}_z. \tag{2.28}$$

Besides, for the charge density $\rho = q \cdot n$, we obtain

$$\rho_p = -n_0 e\frac{\delta n}{n_0}, \tag{2.29}$$

$$\rho_b = -n_0 e\frac{n_b}{n_0}. \tag{2.30}$$

Now dividing the Laplace operator into the parallel and radial directions in cylindrical polar coordinates with respect to the laser propagation axis, i.e. $\nabla^2 = \partial_z^2 + \nabla_\perp^2$, and substituting equation (2.26)-(2.30) into equation (2.25), dividing by the wave-breaking field E_0 through both sides of the equation, we can obtain

$$\left(\frac{1}{c^2}\frac{\partial^2}{\partial t^2} - \nabla_\perp^2 - \frac{\partial^2}{\partial z^2} + k_p^2\right)\frac{\boldsymbol{E}}{E_0} = k_p\left[\frac{1}{c}\frac{\partial}{\partial t}\left(\frac{n_b}{n_0}\right) + \frac{\partial}{\partial z}\left(\frac{\delta n}{n_0} + \frac{n_b}{n_0} - \frac{a^2}{2}\right)\hat{\boldsymbol{e}}_z + \nabla_\perp\left(\frac{\delta n}{n_0} + \frac{n_b}{n_0}\right)\right]. \tag{2.31}$$

And transferring to the comoving frame as what we have done previously, we obtain the deterministic equation for the wakefield in 3D, i.e.

$$\left(\nabla_\perp^2 - k_p^2\right)\frac{\boldsymbol{E}}{E_0} = -k_p\frac{\partial}{\partial \xi}\left(\frac{\delta n}{n_0}\right)\hat{\boldsymbol{e}}_z - k_p\nabla_\perp\left(\frac{\delta n}{n_0} + \frac{n_b}{n_0}\right) + k_p\frac{\partial}{\partial \xi}\left(\frac{a^2}{2}\right)\hat{\boldsymbol{e}}_z. \tag{2.32}$$

Taking the longitudinal part of equation (2.32) and substituting the perturbed density equation (2.22), finally we can get the unified equations for beam and laser-driven plasma wakefield:

$$\left(\frac{\partial^2}{\partial \xi^2} + k_p^2\right)\frac{E_z}{E_0} = -k_p\frac{\partial}{\partial \xi}\left(\frac{\delta n_b}{n_0}\right) - k_p\frac{\partial}{\partial \xi}\left(\frac{a^2}{2}\right). \tag{2.33}$$

2.2.4 Solution for laser-driven wakefield

Solving the equation (2.33) without a beam ($n_b = 0$) yields the following expression for the laser-driven wakefield E_{zl} in the linear limit [10], i.e.

$$\frac{E_{zl}(\xi, r, s)}{E_0} = -k_p^3\int_\infty^\xi d\xi' \cos\left[k_p(\xi - \xi')\right] a^2(\xi', r, s)/4. \tag{2.34}$$

The laser pulses are usually linearly polarized Gaussian envelopes, i.e. the normalized vector potential is of the form $a^2(\xi, r) = a_0^2\exp(-\xi^2/\sigma_l^2)\exp(-2r^2/r_w^2)$, where σ_l and r_w are laser length and waist, respectively. The waist is usually chosen to be $r_w = \pi/k_p$. Considering the condition that $r \gg r_w$, the radial part of the laser strength can be approximated as $a^2(r) \approx (1 - 2r^2/r_w^2)$. In LPA, dephasing is a significant problem for continuous acceleration process, which is also a key point in a beam dump. Dephasing means that the beam might overshoot the laser, since $\gamma_0 \gg \gamma_g$ where γ_0 represents relativistic factor of the beam and γ_g is associated with the laser group velocity v_g. The phase slippage between the beam and the laser is $\Delta\psi \sim k_p s(\beta_0 - \beta_g) \simeq k_p s/2\gamma_g^2$ [10], where β represents the ratio of v to c. Besides, the relative phase between the beam and laser is defined as ψ_0, such that, for $\psi_0 = 0$, the tail of the beam is positioned as $\xi = 0$. The optimized choice for energy extraction is that the tail of the beam should be positioned at the beginning of a decelerating phase as well as a transversely focusing regime of the wake. Under the considerations discussed above, the laser-driven wakefield can be expressed as the oscillation in the form listed below

$$\frac{E_{zl}(\xi, r, s, \psi_0)}{E_0} = \frac{E_{zl}^{max}}{E_0}\sin\left[k_p\xi + \frac{k_p s}{2\gamma_g^2} + \psi_0\right]\left[1 - 2\frac{r^2}{r_w^2}\right], \tag{2.35}$$

where E_{zl}^{max}/E_0 is the wake amplitude. For a Guassian laser pulse, under the linear resonance condition where $\sigma_l = \sqrt{2}/k_p$, where the laser pulse length has the optimal dimension regarding exciting the highest wakefield amplitude, it can be computed as [15]

$$\frac{E_{zl}^{max}}{E_0} \simeq \frac{0.38a_0^2}{(1+a_0^2/2)^{1/2}}. \tag{2.36}$$

The relativistic gamma factor related to the laser group velocity in 1D can be calculated by the equation [16]

$$\gamma_g \simeq k_0/k_p(1+0.051a_0^2), \tag{2.37}$$

where $k_0 = 2\pi/\lambda_0$, λ_0 is laser wavelength. When considering 3D geometry, the correction to γ_g should take into account the contributions from plasma channel and plasma wave-guiding which will be discussed later, thus

$$\gamma_g \simeq k_0/k_p(1+0.051a_0^2)(1+4/r_w^2). \tag{2.38}$$

Therefore, knowing the laser strength, laser wavelength, waist, and the intial relative phase, the laser-driven wakefield can be obtained.

2.3 Enery loss function in active PBD

The axial superposed wakefield driven by the laser and the beam is therefore $E_z/E_0 = (E_{zb} + E_{zl})/E_0$. According to the discussion in the previous report on the energy loss function which is derived from the work done by the electric field, the extended form for the total field is [15]

$$\begin{aligned}&\frac{U(s,\psi_0)}{U_0} = \\ &1 - k_p s\frac{\int_V dV\,[E_{zb}(\xi,r)/E_0]\,[n_b(\xi,r)/n_0]}{\gamma_0\int_V dV n_b(\xi,r)/n_0} - k_p s\frac{\int^s ds'\int_V dV\,[E_{zl}(\xi,r,s',\psi_0)/E_0]\,[n_b(\xi,r)/n_0]}{\gamma_0\int_V dV n_b(\xi,r)/n_0}.\end{aligned} \tag{2.39}$$

The integrals are integrated with respect to the beam volume, where $dV = rdrd\xi$.

Assuming the longitudinal half-sine and transverse parabolic profile, represented by equation (2.4), the energy loss function can be computed through equation (2.39). If simplifying to 1D case, the result is [15]

$$\begin{aligned}\left[\frac{U(s,\psi_0)}{U_0}\right]_{HS} = &\\ 1 - k_p s\frac{k_p L\pi^3(n_b/n_0)(1+\cos(k_p L))}{2\gamma_0(\pi^2 - k_p^2L^2)^2}&\\ - \frac{4\pi^2\gamma_g^2 E_{zl}^{max}/E_0}{\gamma_0(\pi^2-k_p^2L^2)}\cos\left[\frac{k_pL}{2}\right]\sin\left[\frac{k_ps}{4\gamma_g^2}\right]\sin\left[\frac{k_pL}{2}+\psi_0+\frac{k_ps}{4\gamma_g^2}\right].&\end{aligned} \tag{2.40}$$

The full 3D result is too complicated to be listed here. It can be seen that adding laser pulses will help to decelerate the particles faster because of additional laser-related term in equation (2.40). This is also the advantage of active PBD. Besides, due to the dephasing, the laser term also changes the linear trend of total beam energy loss. In this case, whether saturation would occur will be evaluated in simulations.

2.3.1 Application to EuPRAXIA

The EuPRAXIA is an EU study aiming to provide a experimental design for the world's first 1-5 GeV plasma accelerator with industrial-level beam quality [17]. The typical electron bunch, laser pulse and plasma parameters for EuPRAXIA are listed in table 1, which is also what we use in the examination of the capability of active PBD. For the sake of comparison between the active and passive schemes, the beam and plasma parameters here are set to be the same as what we did in the previous report. In the discussions of the active scheme, we will use an electron beam with a half-sine shape, represented by equation (2.6), instead of the Gaussian shape to obtain more compact analytical expressions, under the proper matching condition as

described in the equation (2.5), which gives the value of the longitudinal beam size L. While the transeverse beam size r_b is set to be equal to the longitudinal size. For the laser pulse, the conditions for its length σ_l and waist r_w are set for the sake of obtaining a strongest wakefield amplitude.

Parameter	Value
Beam Energy e_k/GeV	1
Beam Charge Q/pC	30
Beam Length σ_ξ/μm	2
Beam Width σ_r/μm	1.4
Beam Initial Emittance	1%
Beam Size L/μm	7.8
Laser Strength a_0	1
Laser Duration $k_p\sigma_l$	$\sqrt{2}$
Laser Waist $k_p r_w$	π
Laser Wavelength λ_0/μm	0.8
Plasma Density n_0/cm^{-3}	9.9×10^{17}

Table 1: EuPRAXIA parameter

For the simplification of calculations, firstly we start with the 1D geometry, i.e. just considering the longitudinal wakefield effects as well as energy extraction. The half-sinusoidal shape beam will excite a wakefield expressed by equation (2.6), and together with the laser-driven wakefield expressed by equation(2.35) to produce the superposed electric field. The beam-driven, laser-driven and net wakefields in the vicinity of electron beam is depicted in figure 3(a). And the extended view is shown in figure 3(b). The initial phase difference between the beam and the laser is set to $\psi_0 = -0.364425$. In this case, it can achieve the most flat wakefield inside the beam, aiming to extract the energy of the beam in the most uniform way. Even though other values, such as $\psi_0 = 0$, can have a larger wakefield which related to a shorter decelerating distance, preventing energy loss saturation thus to extract all energy is more important. In realistic experiments, there will be no much difference between the 4 cm and 10 cm long plasma channel on experimental installation, but the residual energy in the beam will set requirements on additional conventional beam dump piece. That's the main reason why we choose to have the most flat wakefield instead of the largest one.

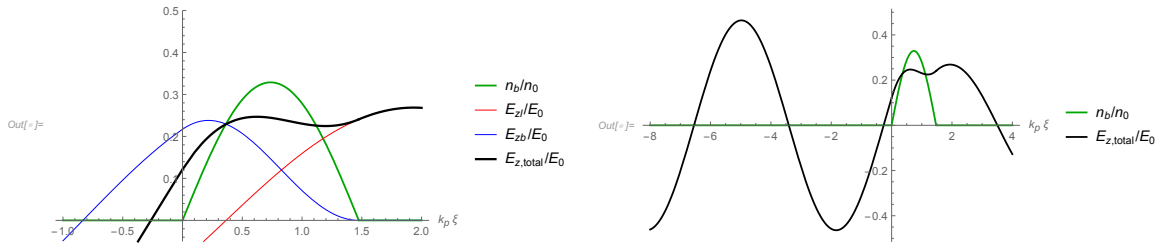

(a) (b)

Figure 3: Beams and their respective wakefields under EuPRAXIA parameters with the initial phase $\psi_0 = -0.364425$. (a) shows longitudinal distribution of one-dimensional normalized half-sine beam density and the self-driven, laser-driven as well as the superposed wakefields in theoretical prediction. (b) shows the extended picture of the beam and total wakefield distributions.

Using the equation (2.40) for total energy loss, we can draw the energy evolution in the active scheme under the parameteres of EuPRAXIA in figure 4(a) in the 1D case. It takes 3.0 cm to extract all energy of the beam, and is shorter than the 7.5 cm of the passive scheme drawn in figure 1(b). Then with the corrections for the γ_g as in equation (2.38) as well as the electric charge, the energy loss in the 3D axisymmetric case is also obtained and shown in figure 4(b). It takes 1.9 cm for the beam to lose all its energy. Therefore, the 3D case displays a higher decelerating gradient than the 1D case.

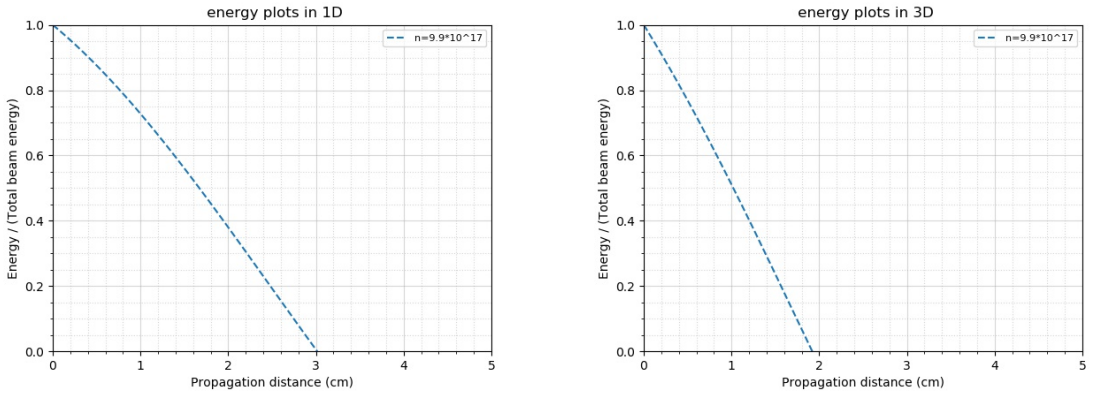

(a) (b)

Figure 4: The energy loss of the half-sine shape beam in EuPRAXIA, where (a) is 1D case and (b) is 3D case.

2.3.2 Application to BNL

The Accelerator Test Facility (ATF) in Brookhaven National Laboratory (BNL) is a proposal driven facility that provides users with high-brightness electron bunches and laser pulses [18]. The specialization in BNL is that it utilizes CO_2 laser, which contains a much larger laser wavelength, usually with 10 μm compared with the usual 0.8 μm from Ti: sapphire lasers which is what EuPRAXIA adopts. The plasma bubble volume driven by the laser scales with the wavelength λ_0. For this reason, a bubble from a CO_2 laser can accommodate a bigger beam, making the deceleration process a little less complex and thus more useful as a longer beam can also be applied. The BNL parameters we use in our active PBD discussion is listed in table 2. Compared to the 1GeV discussed in EuPRAXIA, the initial energy of the beam is set to be relatively small because we need to limit ourselves from the linear to the quasi-linear regime where the laser intensity $a_0 \lesssim 1$. Since the CO_2 lasers have a relatively larger wavelength and thus the beam length can be larger, too. But the beam should still be left with room to fit itself inside the wake, and that is the reason why we would not extend the beam longitudinally too much.

Parameter	Value
Beam Energy e_k/MeV	200
Beam Charge Q/pC	200
Beam Length σ_ξ/μm	10
Beam Width σ_r/μm	10
Beam Size L/μm	39.4
Laser Strength a_0	1
Laser Duration $k_p\sigma_l$	$\sqrt{2}$
Laser Waist $k_p r_w$	π
Laser Wavelength λ_0/μm	9.8
Plasma Density n_0/cm^{-3}	2.5×10^{16}

Table 2: BNL parameter

With the same discussion process as in the previous sub-section, the longitudinal wakefields for BNL paramters are shown in figure 5. The initial phase is set to be $\psi_0 = -0.452389$ for the sake of a relatively flattend wakefield inside beam. Therefore, the energy loss for a BNL beam in active PBD is obtained and drawn in figure 6. It takes 3.99 cm to lose all energy in 1D, and takes 3.21 cm to lose all energy in 3D. It shows the same behaviour that in 3D case the beam energy is lost faster than the 1D case. This might because the work done by beam-driven wakefield in 3D case is greater than the 1D case. Even though the laser-driven

wake decelerates the electrons slower in 3D case, the work efficiency produced by beam-driven wake is more intensive than the 1D behaviour, which might result in the faster total energy extraction.

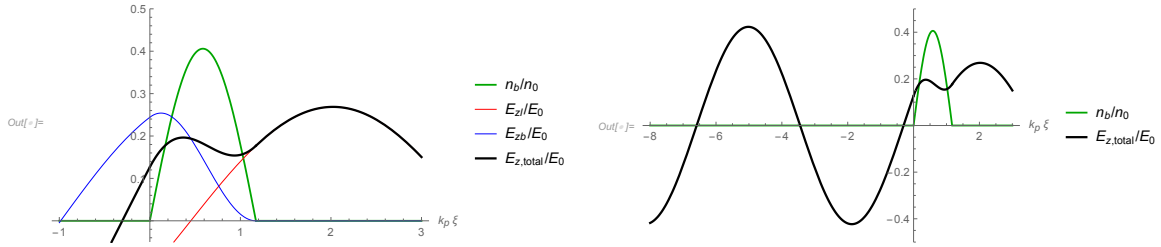

(a) (b)

Figure 5: Beams and their respective wakefields under BNL parameters with the initial phase $\psi_0 = -0.452389$. (a) shows longitudinal distribution of beam density and wakefields while (b) is the extended picture.

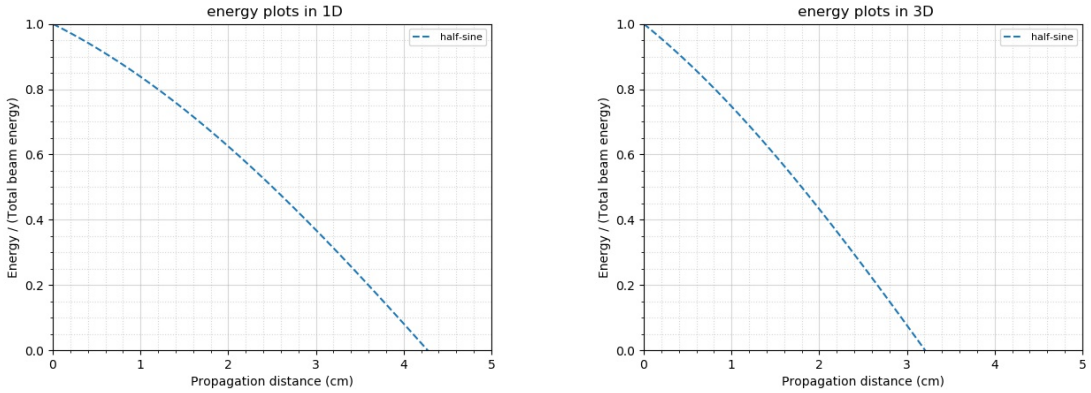

(a) (b)

Figure 6: The energy loss of the half-sine shape beam in BNL, where (a) is 1D case and (b) is 3D case.

In conclusion, in the discussions of the active PBD in the theoretical model and its applications to EuPRAXIA and BNL, we can see that the energy extraction is faster than the passive scheme due to the greater net wakefield along its extension. Besides, the search on a flattened decelerating gradient along the beam is beneficial to obtain the final bunch with less chirp than in passive PBD. Also, the energy stored in the head of the beam is mostly depleted thanks to the preformed laser-driven wake. These compensate for the limitations of the passive scheme and are also the advantages of the active scheme.

2.4 Limitations to active PBD and corresponding solutions

The analytical model is established on the assumption that the laser and the beam will not evolve during the propagation process, which is usually not true in simulations and experiments. The laser-driven wakefield will face with the "3D" vital constraints, i.e. dephasing, diffraction, and depletion. Depletion means that the laser intensity will decrease as it interacts with the plasma. This will be solved with the adoption of multi-staging, which might not be a vital point in a PBD.

For the dephasing problem, we have discussed the causality of it before. The dephasing length is positively related to the plasma wavelength and inversely proportional to the laser wavelength [11]. Dephasing

is also related to the laser propagating velocity, which is represented in the relativistic gamma factor of laser group velocity γ_g which has a relationship to the laser waist. Therefore, to decelerate the beam entirely, the dephasing should be set to occur after the energy extraction completion. The first method is to increase the laser waist to decrease the γ_g, but this would relate to the operation on changing the laser parameters, which is not very convenient in settled experiments. The other method is to lower the plasma density to extend the plasma wavelength and accordingly the dephasing length. Even though the wakefield will be a little bit weaker due to the reduction in the number of plasma electrons, the energy extraction completion is more vital in a PBD. In addition to the dephasing problem, another point to consider is the match of the beam into the total wakefield, and that is also the reason why we cannot adopt a relatively-high density profile of the plasma.

Diffraction means that the laser pulse will only propagate a finite distance before not being able to keep the beam radius small enough to yield the requisite high intensity. In other words, the laser will evolve automatically to the undesirable direction if without external operations. One key factor that determines how long the laser pulse can propagates in the plasma is the Rayleigh length, which represents the distance over which the laser intensity can be maintained. It is defined as [11]

$$z_R = \frac{\pi w_0^2}{\lambda_0}, \tag{2.41}$$

which is where the laser intensity halves. Rather than changing the laser parameters to extend the Rayleigh range itself, there are other methods to support the laser to travel several Rayleigh lengths. In LPA, scientists will often take the relativistic self-focusing effect into account to guide the laser when its power exceeds a critical power [19] as well as using the preformed plasma channel or capillaries. However, in PBD, we should constrain in the linear regime and also don't want to exploit great laser energy consumption, thus the relativistic self-focusing is out of our consideration. Instead, a preformed plasma-density channel is used in PBD design to guide the laser. The mechanism is similar to a gradient-refractive-index optical fibre, where the plasma density is smaller on-axis while larger off-axis. Therefore, the propagation of the laser wavefront is slower than that along the channel boundary, flattening the originally curved laser wavefront. Thus, the entire laser pulse can travel longer than one Rayleigh length while avoiding the diffractive breakup.

In our project, a transverse parabolic density channel of the form $n = n_0 + \Delta n \cdot r^2/r_w^2$ is adopted, while the density in the longitudinal direction remains uniform. The laser propagation is matched to the given parabolic profile in order to mitigate the diffraction [15]. $\Delta n = n(r_w) - n(0)$ is the difference between the density of the laser waist and the central axis, called the channel depth. Therefore, for a laser with low power and intensity, the effective index of refraction is

$$\eta_r = 1 - \frac{\omega_p^2}{2\omega^2}\left(1 + \frac{\Delta n}{n_0}\frac{r^2}{r_w^2}\right), \tag{2.42}$$

where ω is the laser frequency [15]. Considering the Gaussian beam guided at the matched beam spot size, the critical channel depth is calculated to be

$$\Delta n_c = (\pi r_e r_w^2)^{-1}, \tag{2.43}$$

or $\Delta n_c(\mathrm{cm}^{-3}) \simeq 1.13 \times 10^{20}/\mathrm{r_w^2}(\mu\mathrm{m})$, where $r_e = e^2/m_e c^2$ is the classical electron radius [15]. Thus, with the preformed plasma channel, the assumption of a non-evolving laser as we discussed before can be matched.

3 Simulation results

In the establishment of analytical model, we have assumed non-evolving laser and beam behaviours. However, whether the saturation of energy loss and thus the formation of a re-accelerating peak will occur, as well as the problems of laser dephasing and diffraction problems, should be evaluated in simulations. To further investigate the active PBD, FBPIC code is used to simulate the laser-plasma and beam-plasma interactions. This code adopts a spectral solver, which uses a set of 2D radial grids, each of them representing an azimuthal mode [9], but all particles are placed in a 3D cartesian space. In the passive scheme simulations, we used the zero mode (m=0) to denote the axisymmetric fields. Additional modes are used to represent departures from the cylindrical symmetry. Thus, in the active PBD discussions, the first mode $m = 1$ is employed. Simulations with laser usually require a finer grid, in order to properly resolve the laser wavelength. It is even more complicated due to the existence of dephasing and diffraction problems. These make active PBD simulations more computationally expensive. All the discussions are limited in the linear regime where $a_0 \simeq 1$, thus being able to be compared with the analytical model we established in the last chapter. If the laser intensity is higher, for example $a_0 = 4$, nonlinear Thomson scattering will occur between the laser pulse and the electron beam, and synchrotron radiation will be generated [20], which is beyond this report. Our numerical discussions give a preliminary direction of further research and enhancement.

3.1 Plasma channel setup

Diffraction is a key limitation of laser-driven wake propagation and shape retention. In order to guide the laser to several Rayleigh lengths, a plasma channel is established in the simulation. The plasma density distribution is parabolic in the transverse direction and uniform in the longitudinal direction, as depicted in figrue 7. According to equation (2.41), applying the EuPRAXIA parameters from table 1, the channel depth is calculated to be $\Delta n \simeq 0.38 n_0$ at the laser waist $r_w = 16.8$ μm.

The Rayleigh length for EuPRAXIA parameters are calculated to be $z_R = 1105$ μm from equation (2.40). To check whether the guiding is effective, i.e. whether the laser maintains its shape inside a plasma channel as it travels, we can investigate the evolution of the laser envelope as well as peak strength, waist and duration. The laser envelope is shown at the beginning of the simulation (s = 0), and at a later propagation distance, $s \simeq 3600$ μm (which is equivalent to triple Rayleigh lengths) in figure 8, which are roughly the same. This means that the laser pulse has propagated three Rayleigh lengths without suffering diffraction. The laser envelope peak, pulse length, and waist evolution with the propagation distance are drawn in figure 9. Their behaviors exhibit some kind of oscillation, but this is still in expectation since the matching is never perfect. It is approximately uniform as the laser propagates. If without the plasma channel, usually the laser waist would approximately double in one Rayleigh length. Hence, the simulations shall be comparable with the theoretical predictions with the assumption of a non-evolving laser pulse.

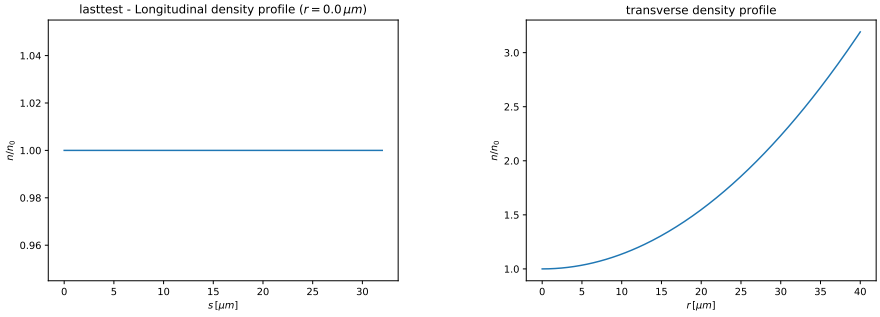

(a) (b)

Figure 7: Plasma electron density distributions is uniform in (a) longitudinal and parabolic in (b) transverse direction in the plasma channel under the EuPRAXIA parameters.

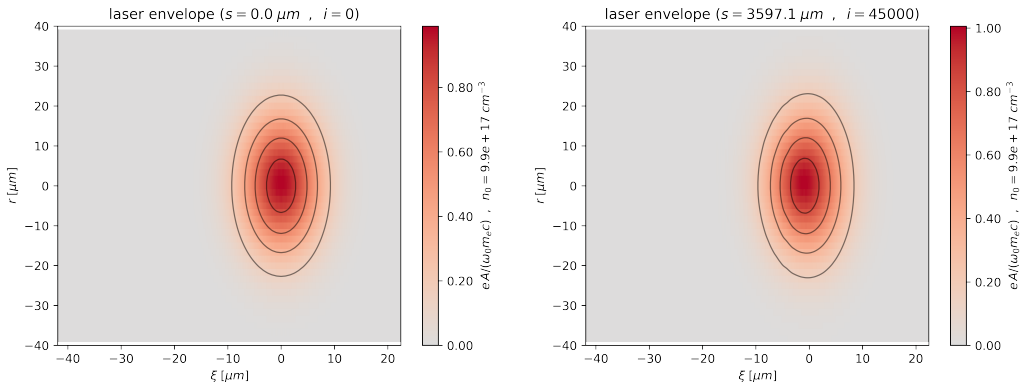

(a) (b)

Figure 8: Laser envelope at the position (a) $s = 0$, (b) $s = 2597.1\mu$m

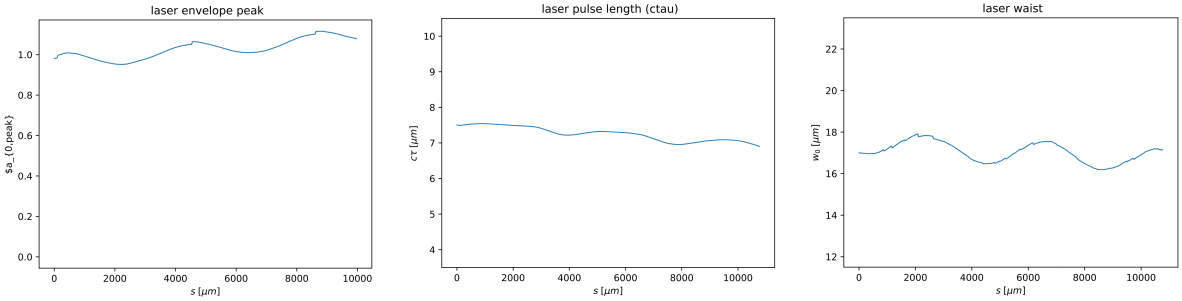

(a) (b) (c)

Figure 9: Evolution of (a) laser envelope peak, (b) laser pulse length, (c) laser waist along s.

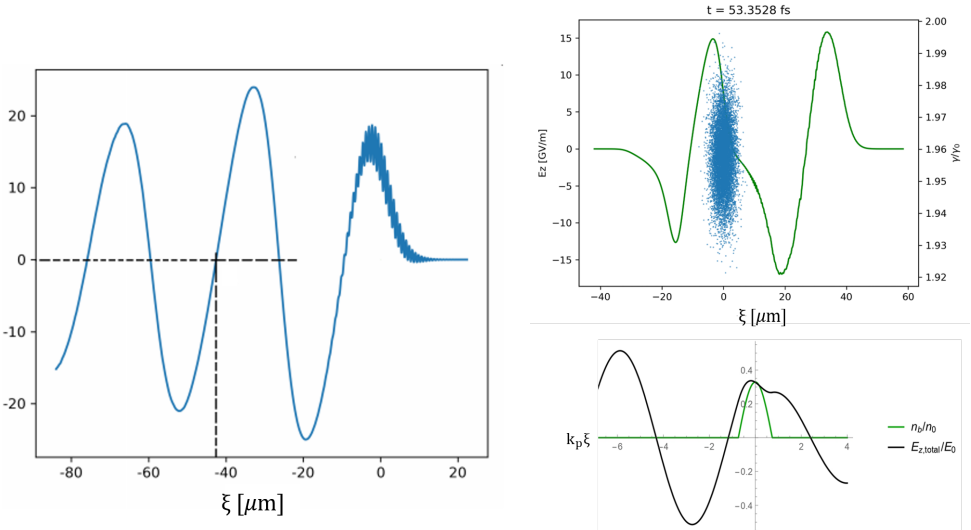

(a) (b)

Figure 10: Wakefields in EuPRAXIA test when $\psi_0 = 0$. (a) Laser-driven wakefield with the laser centroid placed at the origin. (b) Net wakefields with the beam placed at the origin, where the top one is the simulation with the blue dots representing the electrons in phase space, while the bottom is the theoretical prediction.

3.2 Wakefield excitation with zero initial phase

Firstly, we look at wakefield excitation in the EuPRAXIA case with parameters listed in table 1. A linearly polarized Gaussian laser pulse is injected into a preformed plasma channel, and thereafter a 3D Gaussian beam is injected with the zero initial phase difference with respect to the laser-driven wakefield, i.e. $\psi_0 = 0$. In other words, the beam tail is aligned with the start of the laser-driven wake acceleration phase. The purpose is to ensure that the beam is entirely fitted into the decelerating phase to lose its energy. Since the deceleration or acceleration phase depends on the net wakefield, the initial phase close to 0 can also be used to extract energy though.

The purely laser-driven and net wakefields are depicted in figure 10 through simulations. To clarify the position of the beam relative to the laser centroid, we choose the opposite way of thinking. In the figure 10(a), the laser centroid is set at the position $\xi = 0$. Then, Δz, the distance between the laser pulse centroid (origin) and the point of the end of decelerating phase, is about 43 μm. Thereafter, set the beam center to be located in the origin in the comoving frame as drawn in figure 10(b). While the beam length is approximately $L_b \simeq 5\sigma_\xi$, the laser centroid should be placed at the relative distance $\Delta z' = \Delta z - L_b/2 \simeq 37$ μm away from the origin. Through this method, the positions of beam and laser under the condition that $\psi_0 = 0$ are settled. From the comparison with the analytical result obtained from chapter 2, the wake shape inside the beam is flattened a bit due to the superposition of the beam-driven and laser-driven wake, which shows similar behaviours in simulation and theory.

3.3 Energy loss

Under all considerations of the initial phase difference ψ_0 and the set up of the plasma channel as discussed above, the simulations of laser-plasma and beam-plasma interactions can be represented and subsequently the energy extraction in the active PBD with EuPRAXIA parameters, showing in figure 11.

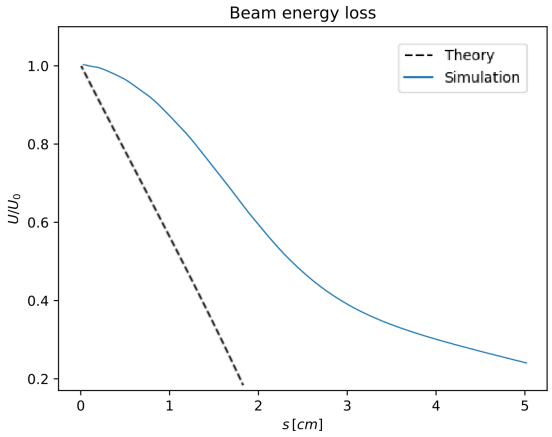

Figure 11: Simulation result and theoretical estimate of beam energy loss in EuPRAXIA with the initial phase $\psi_0 = 0$.

There is a large difference between the simulation result and the theoretical prediction. The most significant difference is the slope of both cases. In the simulation, it takes a distance approximately twice the distance to extract the beam total energy if compared to the analytical estimate. After investigating the possible causes for the observed difference, it was observed that the adopted resolution for the simulation was not fine enough to describe the laser dynamics with the required precision. The numerical parameters we adopt are listed below: grid points in r direction is $N_r = 57$ and in z direction is $N_z = 1256$; resolution is $dz = 8 \times 10^{-8}$, $dr = 7 \times 10^{-7}$; number of particles per cell in r direction is $p_r = p_z = 4$. These parameters are not enough for the entire discussions where the minimum representations of laser scale should be satisfied for scanning. Since higher resolution always means a greater time, the number of grids we used in simulations is smaller

than the requirement due to the relatively compact time we left. Therefore, some messages have been lost in the process, leading to the mismatch between the electron positions and energies. Another explanation might come from the changing relative distance of beam and laser evolutions with the time. As the laser pulse propagates in the plasma, it will lose its energy during the interactions with plasma electrons, therefore it will move backward with respect to the beam, i.e. the dephasing will occur. Thus, after a certain propagation distance, some of the electron bunch will fall behind into the accelerating phase, leading to the total energy extraction slower. Even though it contradicts the analytical estimate in the decelerating gradient, it has revealed the decreasing trend of the total energy of the beam, demonstrating the possibility of active PBD numerically in the overall situation.

In the theoretical analysis, the significance of initial phase difference between the beam and the laser has been emphasized. In FBPIC simulations, we use the relative distance between the laser and the beam instead to represent the phase. By multiplying the laboratory frame distance Δd by the plasma wave number k_p to obtain the phase in the co-moving frame ψ_0, the conversion can be completed. We choose the value of the interval Δd as 0, 10, 20, 30, 40 μm, and then obtain the energy loss plot accordingly as depicted in figure 12(a). The simulations are truncated at $s \sim 1$cm. The green line, corresponding to $\Delta d = 20\mu$m, is the same as $\psi_0 = 3.744$. Looking back to the wakefield, under this initial phase difference, the electron bunch would witness the net accelerating wake, leading to its energy gain. The speeds of energy extraction in other cases can also be explained by the wakefield amplitudes as shown in figure 12(b). In other words, the simulation energy evolution results are consistent with the analytical estimates of the wake.

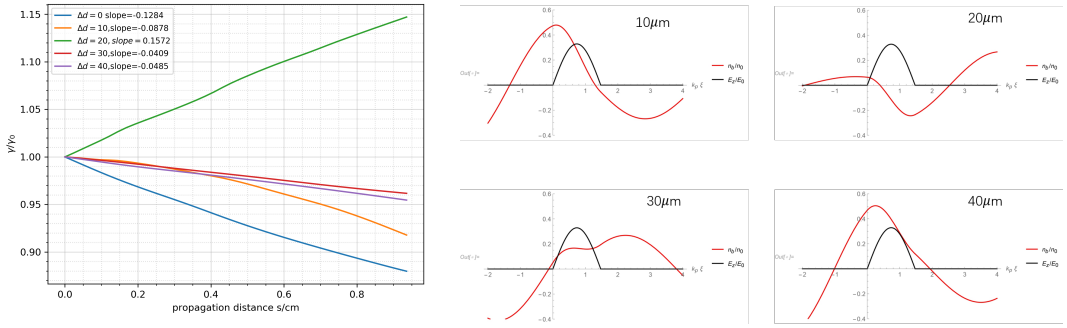

(a) (b)

Figure 12: (a) Energy losses with respect to the various Δd in flat plot and (b) the corresponding wake distributions from theoretical predictions.

4 Conclusions

The project is completed in cooperation with Ziqian Xiang and under the supervision of Dr. Guoxing Xia and Dr. Alexandre Bonatto. Ziqian mainly contributes to the simulation work while I focus on theoretical model establishement. The overall work is done through discussion and intersection.

In this report, we have continued the work on the passive plasma beam dump and extended to the active scheme. The theoretical model has been established using the laser-plasma interaction theory, and perturbation theory with the assumption of a non-evolving laser pulse and electron beam. Unified wakefield expressions for both laser-driven and beam-driven and energy loss functions have been derived and applied to the EuPRAXIA and BNL parameters. It is shown that in the active scheme, the amplitude of the wakefield is larger than the passive scheme, and can also reduce the energies of electrons positioned at the beam head. Besides, by choosing the initial phase difference between the beam and laser, we tried to find the most flattened wakefield and thus the uniform energy extraction. The 3D limitations of laser-driven wakefield based accelerators or decelerators have also been discussed as well as the solutions. Then we have used FBPIC code to simulate the beam energy evolution in the active PBD using EuPRAXIA parameters. Although differences were observed between analytical and numerical results, this might have been caused by the adopted resolution, which was limited by both GPU memory and computational time. But it has represented an energy loss trend, demonstrating that the active PBD is working. The effects of initial phase differences are also evaluated numerically, showing an agreement with the theoretical wake phase relationships, respectively. The evaluation in this report has shown the possibility of exploiting an active PBD to decelerate charged particles in a very short distance uniformly with high efficiency. It has presented a promising insight for further tests on the feasibility and enhancement of the active plasma beam dump.

Acknowledgement

We express gratitude to Dr.Alexandre Bonatto for his tremendous support and advice throughout this project, Dr. Guoxing Xia for his constructive guidance, and Linbo Liang for his help in installing the simulations. Simulation works are carried out on the CSF3 [22] at the University of Manchester and SCARF at the STFC [23], and we express thankfulness for the access they granted us. We also appreciate the work done by all NHS staff and key workers during the coronavirus outbreak.

References

[1] C. Amsler et al., Phys. Lett. B 667, 1 (2008); A. Ferrari et al., CERN-2005-10, INFN/TC-05/11, SLAC-R-773, 2005; G. Battistoni et al., in Proceedings of the Hadronic Shower Simulation Workshop 2006, Fermilab, edited by M. Albrow and R. Raja, AIP Conf. Proc. No. 896 (AIP, New York, 2007), p. 31.

[2] Satyamurthy et al. Design of an 18 MW vortex flow water beam dump for 500 GeV electrons/positrons of an international linear collider. *Nuclear Instruments and Methods in Physics Research, Section A: Accelerators, Spectrometers, Detectors and Associated Equipment*, 679:67–81, 2012.

[3] Satyamurthy et al. Design of an 18 MW vortex flow water beam dump for 500 GeV electrons/positrons of an international linear collider. *Nuclear Instruments and Methods in Physics Research, Section A: Accelerators, Spectrometers, Detectors and Associated Equipment*, 679:67–81, 2012.

[4] Tajima.T, Dawson.J.M., Laser Electron Accelerator. *Physical Review Letters*, 1979, 43(4): 267–270

[5] Chen.P, Dawson.J.M, Huff.R.W. et al. Acceleration of Electrons by the Interaction of a Bunched Electron Beam with a Plasma, *Physical Review Letters*, 1985, Vol.54(7):693-696

[6] Caldwell.A, Lotov.K. Proton-driven plasma-wakefield acceleration *Nature Physics*, 2009, 5(5):363–367

[7] Ian Blumenfeld, Christopher E.et al. Energy doubling of 42 GeV electrons in a metre-scale plasma wakefield accelerator, *Nature*, 2007,445(7129):741–744

[8] Xueying Wang's MPhys project report in the first semester

[9] Remi Lehe, Manuel Kirchen, FBPIC Users Manual for the Fourier-Bessel PIC codes (https://fbpic.github.io/index.html), Ver. 0.14.0, 2016

[10] A. Bonatto, C. B. Schroeder, J. L. Vay, C. G.R. Geddes, C. Benedetti, E. Esarey, and W. P. Leemans. Passive and active plasma deceleration for the compact disposal of electron beams. *Physics of Plasmas*, 22(8), 2015.

[11] Hooker S.M. Developments in Laser-driven Plasma Accelerators *Nature Photonics*, Oct 2013, Vol.7(10):775-782

[12] Gonsalves A., Nakamura K., Daniels J.et al. Petawatt Laser Guiding and Electron Beam Acceleration to 8 GeV in a Laser-Heated Capillary Discharge Waveguide. *Physical Review Letters*, 2019, Vol.122(8):p.084801

[13] S. M. Hooker, R. Bartolini, S. P. D. Mangles, et al, "Multi-Pulse Laser Wakefield Acceleration: A New Route to Efficient, High-Repetition-Rate Plasma Accelerators and High Flux Radiation Sources," *J. Phys. B* 47 234003 (2014).

[14] Panofsky, W. K. H. ; Wenzel, W. A. Some Considerations Concerning the Transverse Deflection of Charged Particles in Radio-Frequency Fields, *Review of Scientific Instruments*, November 1956, Vol.27(11), pp.967-967

[15] E. Esarey, C. B. Schroeder, and W. P. Leemans. Physics of laser-driven plasma-based electron accelerators. *Reviews of Modern Physics*, 81(3):1229–1285, 2009.

[16] C. Benedetti, F. Rossi, C. B. Schroeder, E. Esarey, and W. P. Leemans, Pulse evolution and plasma-wave phase velocity in channel-guided laser-plasma accelerators, *PHYSICAL REVIEW E* 92, 023109 (2015)

[17] Li, X.; Mosnier, A.; Nghiem, P.A.P. Slice energy spread optimization for a 5 GeV laser-plasma accelerator. *Nucl. Instrum. Meth. Phys. Res. A* 2018 ,909, 49.

[18] Y. Fang, V. E. Yakimenko, M. Babzien, et al. Seeding of Self-Modulation Instability of a Long Electron Bunch in a Plasma, *Phys. Rev. Lett.* 112, 045001, 28 January 2014

[19] Wim Leemans, Eric Esarey, Laser-driven plasma-wave electron accelerators, *Phys. Today* 62(3), 44 (2009); doi: 10.1063/1.3099645

[20] Phillip Sprangle and Eric Esarey, Interaction of ultrahigh laser fields with beams and plasmas, *Physics of Fluids B*: Plasma Physics 4, 2241 (1992)

[21] Bonatto, A.; Xia, G; Nunes, R.;Enery loss of an electron beam with Gaussian density profile propagating in a passive plasma beam dump. In Proceedings of the IPAC'19, Melbourne, Australia, 19–24 May 2019; pp. 3584–3586.

[22] The University of Manchester. The Computational Shared Facility (CSF).

[23] Scientific Computing Application Resource for Facilities (SCARF), High Performance Computing Cluster, Science and Technology Facilites Council (STFC).